NRC Research Press

ARTICLE

Synthesis, characterization, and luminescent properties of two new Zr(IV) metal–organic frameworks based on anthracene derivatives

Jennifer M. Rowe, Erin M. Soderstrom, Jie Zhu, Pavel M. Usov, and Amanda J. Morris

Updated online [12 February 2018]: The license for this article has been changed to the CC BY 4.0 license. The PDF and HTML versions of the article have been modified accordingly.

Abstract: Metal–organic frameworks (MOFs) are crystalline materials constructed from metal ions or clusters, connected by multidentate organic ligands. Herein, we describe the synthesis and photophysical properties of two Zr-based, anthracene-containing MOFs, assembled from 2,6-anthracenedicarboxylic acid (2,6-ADCA and 2,6-MOF) and 1,4-anthracenedicarboxylic acid (1,4-ADCA and 1,4-MOF). The 2,6-ADCA analogue formed a highly crystalline octahedral structure that is isostructural with the well-known UiO-67 frameworks. Incorporation of the 1,4-ADCA ligand, on the other hand, resulted in large rod-shaped crystals. Both MOFs exhibit linker-based luminescence. The excited-state properties of the 2,6-MOF and 1,4-MOF were examined using stead-state diffuse reflectance and emission spectroscopies and time-correlated single photon counting (TCSPC) spectroscopy. The photophysical properties of the MOFs are compared with those of the corresponding ligand in solution.

Key words: metal-organic framework, anthracene, luminescence, photophysics.

Résumé : Les réseaux métallo-organiques (MOF, acronyme anglais pour metal–organic frameworks) sont des matériaux cristallins construits à partir d'ions ou d'agrégats métalliques connectés par des ligands organiques multidentates. Dans le présent article, nous décrivons la synthèse et les propriétés photophysiques de deux MOF à base de Zr contenant des groupes anthracène (2,6-MOF et 1,4-MOF). Ces MOF ont été assemblés à partir de l'acide 2,6-anthracènedicarboxylique (2,6-ADCA) et de l'acide 1,4-anthracènedicarboxylique (1,4-ADCA). L'analogue 2,6-ADCA a formé une structure octaédrique hautement cristalline qui est isostructurale aux réseaux bien connus de type UiO-67. Par contre, l'incorporation du ligand 1,4-ADCA a donné lieu à des cristaux de grande taille en forme de bâtonnets. Les deux MOF ont présenté une luminescence associée aux ligands pontants. Nous avons analysé les propriétés de l'état excité du 2,6-MOF et du 1,4-MOF à l'aide des spectroscopies de réflectance diffuse et d'émission à l'état d'équilibre, et de la spectroscopie de comptage monophotonique à corrélation temporelle. Nous avons également comparé les propriétés photophysiques de ces MOF à celles des ligands correspondants en solution. [Traduit par la Rédaction]

Mots-clés : réseau métallo-organique, anthracène, luminescence, photophysique.

Introduction

In recent years, luminescent metal–organic frameworks (MOFs) have been investigated for a variety of applications, including sensing of small molecules, light-emitting devices, and photocatalysts, as well as bioimaging and drug delivery.[1,2] Different components of a framework and interactions between them can give rise to the luminescent behavior such as metal nodes (lanthanides), aromatic organic ligands, metal-to-ligand charge transfer (MLCT) interactions, ligand-to-metal charge transfer (LMCT) interactions, or from guest species.[2,3] Ligand-based luminescence is particularly advantageous because the optical properties of the material may be fine-tuned via ligand functionalization or postsynthetic modifications[4]. Furthermore, the well-defined crystalline nature of MOF scaffolds affords an excellent platform for studying structure–function relationships.[5]

MOFs assembled from luminescent organic ligands often exhibit similar optical properties to the free ligand. However, these properties are altered to varying degrees due to coordination to the metal, π–π interactions, as well as MLCT or LMCT interactions.[2,6,7] To rationally design luminescent MOFs for specific applications, an in-depth understanding of the excited-state properties of the ligand and the effect of incorporation into a MOF structure is necessary. Herein, two anthracene derivatives, 2,6-anthracenedicarboxylic acid (2,6-ADCA) and 1,4-anthracenedicarboxylic acid (1,4-ADCA), were used to construct the UiO-type Zr-based MOFs, 2,6-MOF and 1,4-MOF, respectively. We recently reported a detailed study of the photophysical properties of these ligands.[8] The addition of two carboxylic acid groups onto the aromatic ring system has a pronounced effect on the behavior of the parent anthracene moiety, which depends on their location and protonation state. The excited state properties of the 2,6-MOF and 1,4-MOF were investigated and compared with those of the free ligand in solution.

Experimental

Materials

2,6-ADCA and 1,4-ADCA were synthesized as previously described and characterized by ^{1}H NMR spectroscopy.[8] All other chemicals and

Received 17 July 2017. Accepted 5 October 2017.

J.M. Rowe, E.M. Soderstrom, J. Zhu, P.M. Usov, and A.J. Morris. Department of Chemistry and Macromolecules Innovation Institute, Virginia Tech, Blacksburg, VA 24061, USA.

Corresponding author: Amanda J. Morris (email: ajmorris@vt.edu).

This paper is part of a Special Issue entitled "2016 Gordon Research Conference on Electron Donor Acceptor Interactions (GRC – EDAI)".

solvents, including $ZrCl_4$, *N,N′*-dimethylformamide (DMF, HPLC grade > 99%), acetic acid (reagent grade > 99%), and formic acid (reagent grade > 99%), were used as received without further purification from Alfa Aesar, Fisher Scientific, or Sigma-Aldrich.

Synthesis of 2,6-MOF

$ZrCl_4$ (23.3 mg, 0.1 mmol) and 2,6-ADCA (26.6 mg, 0.1 mmol) were added to a 2-dram vial along with DMF (5 mL) and formic acid (60 equiv). The vial was capped and sealed with Teflon tape and the mixture was ultrasonicated for 15 min. The vial was then placed in an oven and heated at 120 °C for 24 h. The reaction solution was centrifuged immediately and the solvent was decanted off. The isolated solid was washed with DMF and centrifuged again until the solution was clear. The DMF was decanted off and the solid was dried under vacuum for 3 days.

Synthesis of 1,4-MOF

$ZrCl_4$ (23.3 mg, 0.1 mmol) and 1,4-ADCA (26.6 mg, 0.1 mmol) were added to a 2-dram vial along with DMF (3 mL) and acetic acid (80 equiv). The vial was capped and sealed with Teflon tape and the mixture was ultrasonicated for 15 min. The vial was then placed in an oven and heated at 100 °C for 12 h. The reaction solution was centrifuged immediately and the solvent was decanted off. The isolated solid was washed with DMF and centrifuged again until the solution was clear. The DMF was decanted off and the solid was dried under vacuum for 3 days.

Powder X-ray diffraction (PXRD)

PXRD patterns of MOF samples were obtained using a Rigaku Miniflex 600 with Cu(Kα) radiation (Cu-Kα = 1.5418 Å) in continuous scanning mode (10.0° per min) and a resolution of 0.1° 2θ.

Scanning electron microscopy (SEM)

SEM images were collected with a Leo/Zeiss 1550 Schottky field-emission SEM equipped with an in-lens detector, operating at 5 kV. Le Bail refinement of the 2,6-MOF powder pattern was performed using Rietica for Windows v2.1 software.

Thermogravimetric analysis (TGA)

A Q-series TGA from TA instruments was used to analyze thermal stability of materials. Ten milligrams of sample in a high temperature platinum pan were heated under N_2 from 25 °C to 600 or 800 °C at a heating rate of 10 °C per min.

Gas sorption isotherms

The N_2 sorption isotherm measurements were collected on a Quantachrome Autosorb-1 at 77 K. The samples were placed in a 6 mm large bulb sample cell, which was degassed under vacuum for 24 h at 120 °C. The surface areas of the materials were determined by fitting the adsorption data within the 0.05–0.3 P/P_0 pressure range to the BET and Langmuir equations.

Steady-state absorption spectroscopy

The steady-state absorption spectra of the ligands were obtained using an Agilent Technologies 8453 UV–vis diode array spectrophotometer (1 nm resolution) where the spectra were recorded with samples prepared in a 1 cm quartz cuvette. The same instrument was used to obtain diffuse reflectance spectra of MOF powders, where the sample compartment was replaced with an integration sphere. The powder samples were diluted by mixing with $BaSO_4$.

Steady-state emission spectroscopy and time-resolved emission lifetimes

Approximately 3 mg of MOF powder were suspended in 3 mL DMF and the sample was continuously stirred during the emission measurements. The ligand samples were prepared at concentrations of ~8 μmol/L in DMF. The protonated (ADCA) and deprotonated (ADC^{2-}) ligand samples were prepared in aqueous solutions, using HCl or NaOH to achieve pH values of ~2 and 10.5, respectively. Time-resolved fluorescence lifetimes were obtained via the time-correlated single photon counting technique (TCSPC) with a modified QuantaMaster QM-200-4E emission spectrophotometer from Photon Technology, Inc. (PTI) equipped with a 350 nm LED and a Becker & Hickl GmbH PMH-100 PMT detector with time resolution of <220 ps FWHM. Florescence lifetime decays were deconvoluted from the time-dependent florescence signal and the instrument response function using the fluorescence decay analysis software, DecayFit, available online (Fluortools, http://www.fluortools.com/; Supplementary Figs. S4–S6).

Quantum yields of fluorescence and steady-state emission spectra of the ADCA compounds were measured in DMF. The steady-state emission spectra were obtained using the same QuantaMaster Model QM-200-4E where the sample compartment was replaced with an integrating sphere (PTI). The excitation light source was a 75 W Xe arc lamp (Newport). The detector was a thermoelectrically cooled Hamamatsu 1527 photomultiplier tube (PMT). Kinetic traces were analyzed using Origin.

To ensure stability of the MOF and the absence of free linker, the solutions were syringe filtered and emission was monitored at the maximum wavelength of emission for each ligand after the emission experiments were completed.

Results

Synthesis and characterization of 2,6- and 1,4-MOFs

Synthesis of the 2,6-MOF and 1,4-MOF was adopted from previously reported methods for the UiO-66 framework with minor modifications.[9–11] Briefly, for the 2,6-MOF, 0.1 mmol $ZrCl_4$ and 0.1 mmol 2,6-ADCA were dissolved in 5 mL DMF along with 60 equiv formic acid as the modulator. The mixture was sonicated for 15 min followed by heating at 120 °C for 24 h. To synthesize the 1,4-MOF, 0.1 mmol $ZrCl_4$, 0.1 mmol 1,4-ADCA, and 80 equiv acetic acid were added to 3 mL DMF, the mixture was sonicated for 15 min, and then, it heated at 100 °C for 12 h. The PXRD patterns of the 2,6-MOF and 1,4-MOF are shown in Figs. 1A and 2A, respectively. The diffraction data confirmed the formation of crystalline materials with a relatively large lattice spacing, as indicated by the presence of peaks below 10° 2θ, a telltale sign of framework structures. SEM images (Fig. 1B) revealed that the 2,6-ADCA MOF forms octahedral particles with an average size of ~200 nm. On the other hand, the 1,4-ADCA MOF crystallized into rod-shaped particles, several microns in size (Fig. 2B). The internal surface area of the synthesized frameworks was assessed using N_2 sorption experiment at 77 K. Fitting the data to the BET model gave 711.49 $m^2\ g^{-1}$ surface area with and a pore volume of 14.86 $cm^3\ g^{-1}$ for 2,6-ADCA analogue (Supplementary Fig. S1). The 1,4-MOF, on the other hand, exhibited a BET surface area of 378.09 $m^2\ g^{-1}$ and pore volume of 52.02 $cm^3\ g^{-1}$ (Supplementary Fig. S2). Thermogravimetric analysis of the MOFs revealed that decomposition of the framework occurs at ~450 °C for the 2,6-MOF (Supplementary Fig. S3) and ~500 °C for the 1,4-MOF (Supplementary Fig. S4), as evidenced by a large weight drop due to the ligand breakdown. The initial ~20% weight losses are attributed to the removal of solvent molecules from the pores of the MOF. The remaining percent weights (53% for 2,6-MOF and 26% for 1,4-MOF) correspond to ZrO_2 formed after the decomposition of the anthracene linkers.[12]

Excited-state properties

To examine how the ground- and excited-state properties of the ligands are affected by coordination to Zr^{4+} in the MOF structure, the photophysics of these materials were compared with that of the protonated (ADCA) and deprotonated (ADC^{2-}) ligands in solution. The absorption and emission spectra of the ADCA-based MOFs are shown in Fig. 3 (the respective excitation spectra are shown in Supplementary Figs. S6–S7), along with that of the corresponding protonated (ADCA) and deprotonated (ADC^{2-}) ligands.

Fig. 1. (A) PXRD patterns of the 2,6-MOF (black) compared with the simulated powder pattern of UiO-67 (red) and (B) SEM image of 2,6-MOFs. [Colour online.]

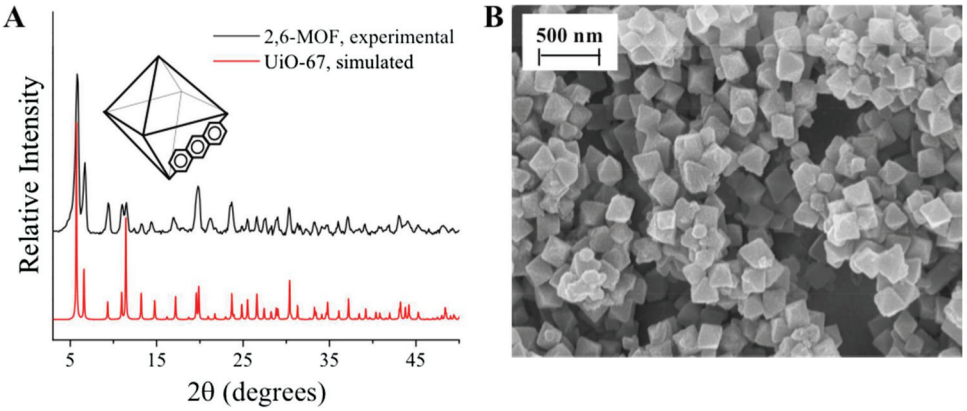

Fig. 2. (A) PXRD patterns of 1,4-MOF (black) compared with the simulated powder pattern of UiO-66 (red) and (B) SEM image of 1,4-MOFs. [Colour online.]

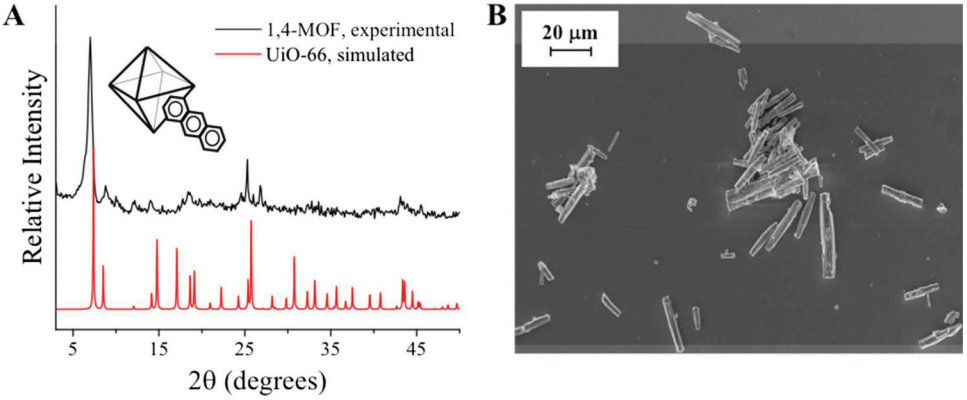

The absorption spectrum of the 2,6-MOF is significantly broadened compared with that of 2,6-ADCA and 2,6-ADC^{2-}, whereas the five sharp absorption bands, observed in the spectrum of 2,6-ADCA, are discernable in the framework spectrum. The 1,4-ADC Zr MOF displays a diffuse absorption spectrum, similar to that of 1,4-ADCA ligand. The absorption spectra of the 2,6-MOF and 1,4-MOFs are redshifted by 4 nm and 7 nm, relative to protonated ligands, and 21 nm and 27 nm, relative to deprotonated forms, respectively.

The emission spectrum of the 2,6-MOF closely resembles that of the protonated, 2,6-ADCA ligand, with similar vibronically structured emission bands, and is only slightly blueshifted by ~2 nm relative to the free ligand. The 1,4-MOF displays a broad emission, with a maximum (λ_{max}) at ~465 nm, in between that of 1,4-ACDA (532 nm) and 1,4-ADC^{2-} (430 nm).

The fluorescence lifetimes and quantum yields of the MOFs were measured from suspensions in DMF and are listed in Table 1 along with the protonated and deprotonated ADCA ligands. The 2,6-MOF exhibited a mono-exponential florescence decay, with a florescence lifetime (τ_f) of 16.6 ± 1.1 ns (Supplementary Figs. S8–S10; Supplementary Table S1) and quantum yield (Φ_f) of 0.87 ± 0.04 comparable with that observed for 2,6-ADCA in solution, and are ascribed to linker-based emission. The 1,4-MOF emission decay exhibits bi-exponential behavior, with different lifetime values obtained for the emission decay at in the higher (~400–450 nm) and lower (~500–550 nm) energy regions of the spectrum (Fig. 4; Table 1). Global analysis of the emission decay yielded lifetime components of τ_1 = 7.5 ± 0.1 ns and τ_2 = 19.9 ± 0.1 ns. The shorter lifetime component, τ_1, lies between that of 1,4-ADCA and 1,4-ADC^{2-}, whereas τ_2 is much longer than the lifetime of either the free 1,4-ADCA or 1,4-ADC^{2-} ligands in solution.

Discussion

Structural characterization of MOFs

The structures of the 2,6-MOF and 1,4-MOF were analyzed by comparing their powder patterns with the well-known UiO-67 and UiO-66 frameworks, respectively, because crystals large enough for single-crystal X-ray analysis could not be obtained.[13,14] The PXRD pattern of the 2,6-MOF is compared with that of UiO-67, in which the octahedral $[Zr_6(\mu_3\text{-}O)_4(\mu_3\text{-}OH)_4]^{12-}$-clusters are capped by 12 carboxylate groups from biphenyl-4,4′-dicarboxylate (BPDC) ligands resulting in an extended cubic structure. It is expected that functionalization of 2 and 6 positions around the anthracene ring system will result in a ligand with a similar length and shape as BPDC (a priori). The peaks observed in the powder pattern of the 2,6-MOF match well with the simulated PXRD patterns UiO-67. Le Bail refinement of the 2,6-MOF data (Supplementary Fig. S5) indicated a UiO-type structure with a unit cell parameter a = 26.97 Å, which correlates with the length of the 2,6-ADCA ligand. The SEM images show that the 2,6-MOFs form the quintessential octahedral-shaped crystals characteristic of UiO structures.

The binding nature for the 1,4-MOF would likely be similar to that of UiO-66, composed of 1,4-benzenedicarboxylate (BDC) ligands. The PXRD pattern obtained for the 1,4-MOF has distinct similarities to that of UiO-66, although it is not a direct match. The PXRD peaks appear broadened, which may indicate that some amorphous material is present. Furthermore, the SEM images show that the shape of the 1,4-MOF is that of large rod-shaped crystals not expected for UiO-66. These differences could possibly be ascribed to a large degree of defects within the crystal caused by the high steric bulk of the 1,4-ADCA ligand within the UiO-type framework.

Fig. 3. Absorption and emission spectra of (A and B) 2,6-ADCA and (C and D) 1,4-ADCA in acidic solution (ADCA, red), basic solution (ADC^{2-}, blue), and incorporated into the MOF (black). λ_{ex} = 390 nm for 2,6-ADCA and 2,6-MOF, 370 nm for 2,6-ADC^{2-}, 400 nm for 1,4-ADCA and 1,4-MOF, and 375 nm for 1,4-ADC^{2-}. [Colour online.]

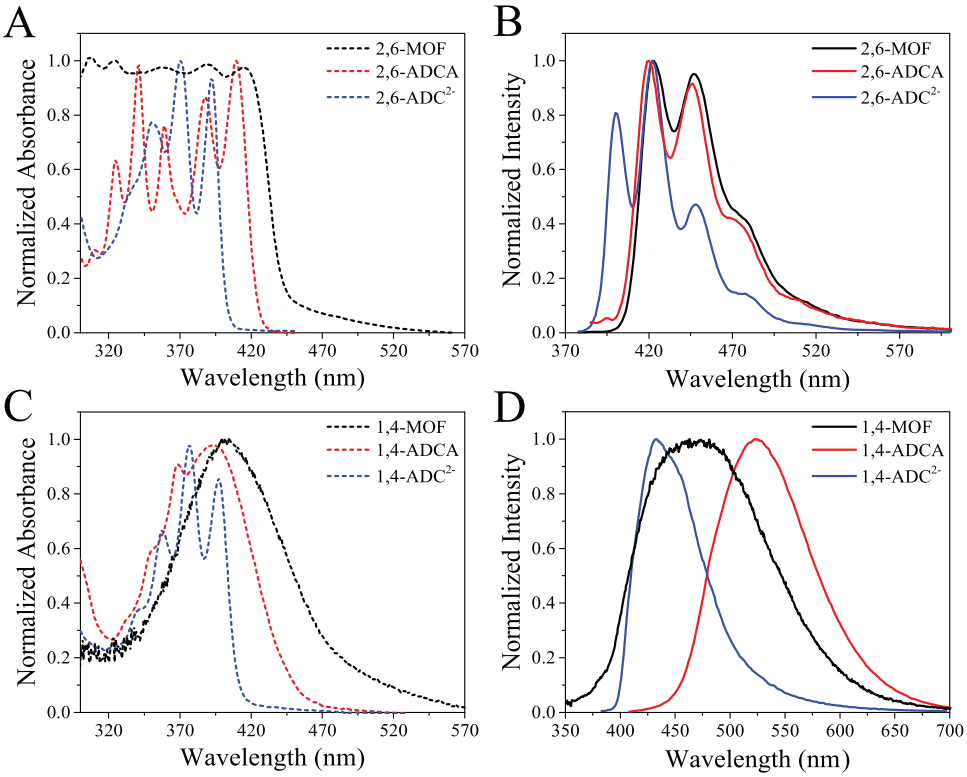

Table 1. Summary of absorption and emission data, fluorescence lifetimes, and quantum yields of the Zr-MOFs and anthracene-based linkers in solution and inside the frameworks.[8]

	$\lambda_{max,abs}$ (nm)	$\lambda_{max,em}$ (nm)	τ_1 (ns)	τ_2 (ns)	Φ_f
2,6-MOF	415	421	16.6±1.1	—	0.87±0.04
2,6-ADCA	410	423	15.2±0.2	—	0.82±0.08
2,6-ADC^{2-}	371	422	6.2±0.05	—	0.11±0.02
1,4-MOF	405	465	7.5±0.1	19.9±0.1	0.002±0.0001
1,4-ADCA	393	550	12.5±0.1	—	0.19±0.04
1,4-ADC^{2-}	377	433	3.5±0.1	—	0.07±0.02

That said, rod-like structures are exhibited by Zr-MOFs including porphyrinic MOFs in the PCN series.[15] Repeated attempts to synthesize higher quality crystals for advanced structural analysis were unsuccessful (Fig. 5).

Excited-state properties

The vibronic structure observed in the absorption spectrum of 2,6-ADCA is attributed to the $^1A_1 \rightarrow {}^1L_b$ electronic transitions, polarized along the longitudinal axis of the anthracene plane. Functionalization of anthracene along this axis, at the 2 and 6 positions, with the electron-withdrawing carboxylic acid groups stabilized these transitions, resulting in the observed intense, vibronically structured $^1A_1 \rightarrow {}^1L_b$ bands.[6] The similar vibronic structure observed in the absorption spectrum of the 2,6-MOF indicates that the $^1A_1 \rightarrow {}^1L_b$ transitions remain stabilized upon coordination into the MOF. The emission spectrum of the 2,6-MOF closely resembles that of 2,6-ADCA in solution. Taken together, the similarity between the vibronic bands in the absorption and emission spectra of the framework and the free ligand reveal that incorporation of the 2,6-ADCA derivative into the MOF has negligible effects on the $^1A_1 \rightarrow {}^1L_a$ transition.

The τ_f and Φ_f of the 2,6-MOF (τ_f = 16.6 ± 1.1 ns, Φ_f = 0.87 ± 0.04) are very similar to that of 2,6-ADCA (τ_f = 15.2 ± 0.2 ns, Φ_f = 0.82 ± 0.08). They are defined by eqs. 1 and 2, respectively, where k_r is the rate of radiative decay and k_{nr} is the rate of nonradiative decay.[20,21] The slight increase in both the τ_f and Φ_f could be attributed to steric restraint imposed on the chromophore by the MOF scaffold, which reduces nonradiative decay pathways.[7,15,17] The carboxylate functionalities were previously found to display slight resonance interactions with the anthracene unit of 2,6-ADCA, and therefore, rotation of these units resulted in nonradiative energy dissipation in the ligand.[8] The rotation of these functional groups that can occur in dilute solutions is largely suppressed when they are bound to the Zr-oxo clusters.

$$(1) \qquad \tau_f = \frac{1}{k_r + k_{nr}}$$

$$(2) \qquad \Phi_f = \frac{k_r}{k_r + k_{nr}}$$

In contrast to the 2,6-MOF, 1,4-MOF exhibits substantial band broadening and a significant redshift in the observed absorption spectrum. This behavior is indicative of intermolecular interactions (π–π stacking) between the anthracene moieties.[17] The magnitude of the effect of π interactions on the photophysical properties of anthracenes is sensitive to the distance between chromophores, as well as their relative orientation. Considering the short axis of anthracene (7.8 Å) and the size of potential MOF cages in Zr-MOFs, the long axis of 1,4-ADCA (11.8 Å) could potentially protrude into the pore and significantly interact with other anthracenes through a π overlap.[17,19]

Fig. 4. (A) Time-resolved emission spectrum of 1,4-ADCA from 0 ns to 300 ns and (B) monomer (red) and excimer (blue) emission spectra obtained from global analysis of the net (black) emission spectrum. [Colour online.]

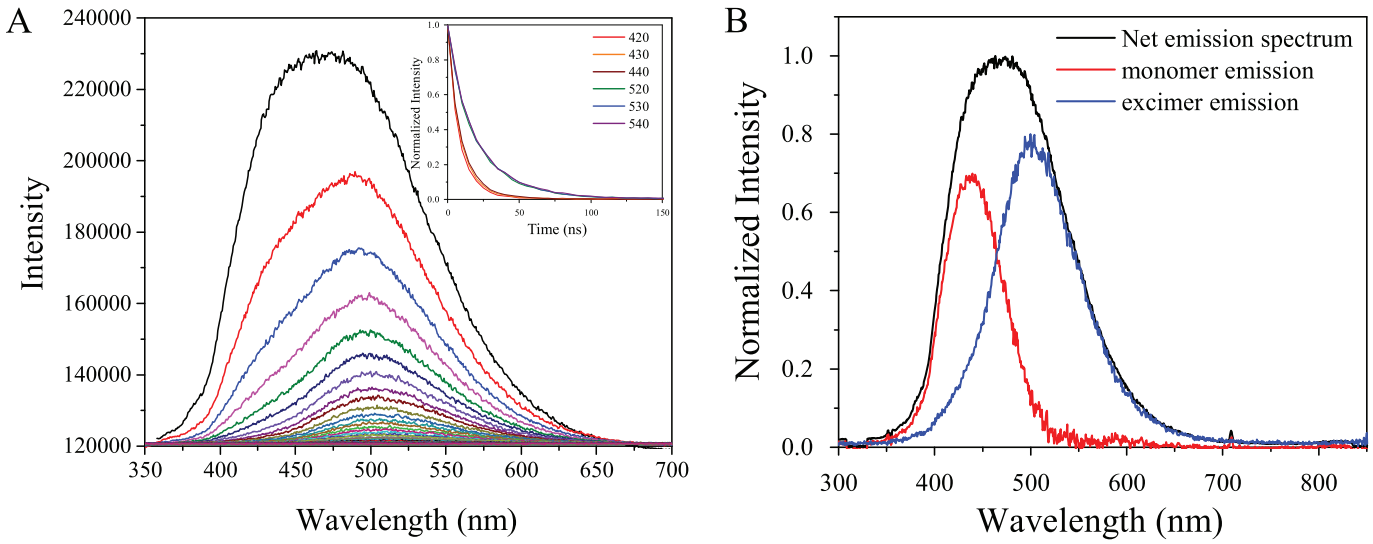

Fig. 5. Cartoon representation of 2,6-MOF and possible 1,4-MOF structures.

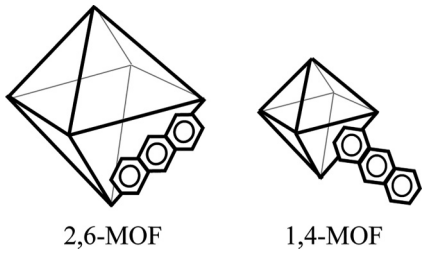

The photoluminescence data for 1,4-MOF also indicate modulation of the photophysical properties upon MOF incorporation, potentially due to π–π interactions. The emission spectrum of 1,4-MOF is significantly broadened and does not resemble that of either protonated or deprotonated free linker (ADCA or ADC^{2-}). Furthermore, the bi-exponential lifetime behavior of the 1,4-MOF emission indicate the presence of two populations of chromophores. Considering the possibilities, the two populations could result from (1) encapsulated vs. incorporated anthracene linkers,[18] (2) perfect vs. defected attachment of linkers within the framework, or (3) monomeric vs. excimer emission.

Global spectral fitting of the emission spectra enables the determination of the unique emission profiles for the two populations (Fig. 4). The population exhibiting the shorter lifetime component (7.5 ± 0.1 ns) resembles the emission profile for 1,4-ADC^{2-}. The observed lifetime is slightly longer than that for 1,4-ADC^{2-}. We previously showed that the excited-state properties of 1,4-ADCA and 1,4-ADC^{2-} are significantly affected by both resonance interactions between the carboxylate groups and aromatic plane and free rotation of these functional groups.[8] Coordination of the ligand at the 1 and 4 positions imposes some steric hindrance that limits rotation of the carboxylates and decreases the associated vibrational relaxation pathways, giving rise to a longer fluorescence lifetime. Therefore, we assign the higher energy (shorter lifetime) population to that of monomeric linker emission.

To assign the longer, lower energy emissive population, the three potential situations enumerated above were considered. Due to the dramatically decreased quantum yield (Φ_f = 0.002 ± 0.0001), the third possibility, excimer formation, is most likely. An encapsulated population would be expected to behave similarly to the protonated free linker in solution. A defect population could resemble either protonated or deprotonated linker with similar lifetime and quantum yield. Although the lifetime observed (19.9 ± 0.1 ns) could potentially be expected for a population resembling ADCA in a rigidified environment, the quantum yield suggests otherwise. Excimer formation is known to result in both an increased lifetime and a decreased quantum yield, as observed here. Additionally, excimers exhibit redshifted emission spectra relative to monomeric emission. Considering the assignment of the shorter lived component to monomeric linker emission, the same trend is observed here (435 nm vs. 503 nm). Additionally, excimer formation has previously been observed in anthracene crystals and also resulted in ground state and (or) static quenching.[8,16] Given the preceding discussion, it is likely that 1,4-MOF forms an excimer between neighboring or adjacent anthracene units facilitated by π–π interactions.

Conclusions

The photophysics of the two anthracene derivatives, 2,6-ADCA and 1,4-ADCA, were shown to be altered upon coordination to the zirconium-based nodes in the two frameworks, 2,6-MOF and 1,4-MOF. The unique fluorescent properties of the ligands, as well as individual framework structure, resulted in distinctive luminescent behavior. The distances between anthracene units and their orientation within the framework dictate the extent of intermolecular interactions. In the 1,4-MOF, where the anthracene units are in the appropriate orientation and proximity to one another, there is efficient π-orbital overlap, giving rise to excimer formation. Whereas in the 2,6-MOF, the anthracene units are spatially separated, and π–π interactions are considerably weaker, and as a result, the emissive properties resemble that of the free linker in solution. The study provides an example of structure dependence of MOF photophysical properties, which is facilitated by through-space interactions between chromophores. Furthermore, it was demonstrated that luminescent properties of a framework can be controlled by the functionalization of appropriate positions around the anthracene moiety.

Supplementary data

Supplementary data are available with the article through the journal Web site at http://nrcresearchpress.com/doi/suppl/10.1139/cjc-2017-0445.

Acknowledgements

This material is based upon work supported by the U.S. Department of Energy, Office of Science, Office of Basic Energy Sciences, under Award Number DE-SC0012446.

References

(1) Hu, Z.; Deibert, B. J.; Li, J. *Chem. Soc. Rev.* **2014**, *43*, 5815. doi:10.1039/C4CS00010B.
(2) Allendorf, M. D.; Bauer, C. A.; Bhakta, R. K.; Houk, R. J. *Chem. Soc. Rev.* **2009**, *38*, 1330. doi:10.1039/b802352m.
(3) Zhu, J.; Shaikh, S.; Mayhall, N.; Morris, A. J. *Elaboration and Applications of Metal–Organic Frameworks*; Imperial College: London, in press.
(4) Inokuma, Y.; Yoshioka, S.; Ariyoshi, J.; Arai, T.; Hitora, Y.; Takada, K.; Matsunaga, S.; Rissanen, K.; Fujita, M. *Nature* **2013**, *495*, 461. doi:10.1038/nature11990.
(5) Lu, W.; Wei, Z.; Gu, Z. Y.; Liu, T. F.; Park, J.; Park, J.; Tian, J.; Zhang, M.; Zhang, Q.; Gentle, T., III; Bosch, M.; Zhou, H. C. *Chem. Soc. Rev.* **2014**, *43*, 5561. doi:10.1039/C4CS00003J.
(6) Meek, S. T.; Greathouse, J. A.; Allendorf, M. D. *Adv. Mater.* **2011**, *23*, 249. doi:10.1002/adma.201002854.
(7) Perry, J. J., IV; Feng, P. L.; Meek, S. T.; Leong, K.; Doty, F. P.; Allendorf, M. D. *J. Mater. Chem.* **2012**, *22*, 10235. doi:10.1039/c2jm16627e.
(8) Rowe, J. M.; Hay, J. M.; Maza, W. A.; Chapleski, R. C.; Soderstrom, E.; Troya, D.; Morris, A. J. *J. Photochem. Photobiol., A* **2017**, *337*, 207. doi:10.1016/j.jphotochem.2016.12.021.
(9) Katz, M. J.; Brown, Z. J.; Colón, Y. J.; Siu, P. W.; Scheidt, K. A.; Snurr, R. Q.; Hupp, J. T.; Farha, O. K. *Chem. Commun.* **2013**, *49*, 9449. doi:10.1039/c3cc46105j.
(10) Pu, S.; Xu, L.; Sun, L.; Du, H. *Inorg. Chem. Commun.* **2015**, *52*, 50. doi:10.1016/j.inoche.2014.12.015.
(11) Schaate, A.; Roy, P.; Godt, A.; Lippke, J.; Waltz, F.; Wiebcke, M.; Behrens, P. *Chem. - Eur. J.* **2011**, *17*, 6643. doi:10.1002/chem.201003211.
(12) Tranchemontagne, D. J.; Hunt, J. R.; Yaghi, O. M. *Tetrahedron* **2008**, *64*, 8553. doi:10.1016/j.tet.2008.06.036.
(13) Valenzano, L.; Civalleri, B.; Chavan, S.; Bordiga, S.; Nilsen, M. H.; Jakobsen, S.; Lillerud, K. P.; Lamberti, C. *Chem. Mater.* **2011**, *23*, 1700. doi:10.1021/cm1022882.
(14) Chavan, S.; Vitillo, J. G.; Gianolio, D.; Zavorotynska, O.; Civalleri, B.; Jakobsen, S.; Nilsen, M. H.; Valenzano, L.; Lamberti, C.; Lillerud, K. P.; Bordiga, S. *Phys. Chem. Chem. Phys.* **2012**, *14*, 1614. doi:10.1039/C1CP23434J.
(15) Kelty, M. L.; Morris, W.; Gallagher, A. T.; Anderson, J. S.; Brown, K. A.; Mirkin, C. A.; Harris, T. D. *Chem. Commun.* **2016**, *52*, 7854. doi:10.1039/C6CC03264H.
(16) Lakowicz, J. R. In *Fluorescence Studies on Biological Membranes*; Hilderson, H. J., Ed.; Subcellular Biochemistry Vol. 13; Springer: Boston, 1988; pp. 89–126. doi:10.1007/978-1-4613-9359-7_3.
(17) Jas, G. S.; Wang, Y.; Pauls, S. W.; Johnson, C. K.; Kuczera, K. *J. Chem. Phys.* **1997**, *107*, 8800. doi:10.1063/1.475172.
(18) Maza, W. A.; Morris, A. J. *J. Phys. Chem. C* **2014**, *118*, 8803. doi:10.1021/jp501140r.
(19) Hong, D. H.; Suh, M. P. *Chem. - Eur. J.* **2014**, *20*, 426. doi:10.1002/chem.201303801.
(20) de Melo, J. S. S.; Costa, T.; de Castro, C. S.; Maçanita, A. L. In *Photochemistry*. Albini, A., Fasani, E., Eds.; Royal Society of Chemistry: Cambridge, UK, 2013; Vol. 41, pp. 59–126. doi:10.1039/9781849737722-00059.
(21) Valeur, B.; Berberan-Santos, M. N. *Molecular Fluorescence: Principles and Applications*, 2nd ed.; Wiley-VCH: Weinheim, Germany, 2012; p. 61. doi:10.1002/9783527650002.
(22) Sugino, M.; Araki, Y.; Hatanaka, K.; Hisaki, I.; Miyata, M.; Tohnai, N. *Cryst. Growth Des.* **2013**, *13*, 4986. doi:10.1021/cg401166v.